Letters

Parameters Uncertainty Immunization of Global Synchronous Pulsewidth Modulated VSIs With Round P&O Algorithm

Tao Xu, *Member, IEEE*, Feng Gao, *Senior Member, IEEE*, Pengfei Tan, Xiangjian Meng, *Student Member, IEEE*, and Frede Blaabjerg, *Fellow, IEEE*

***Abstract*—This letter proposes a closed-loop scheme for global synchronous pulsewidth modulated voltage source inverters with round perturbation and observation (R-P&O) algorithm to immunize the parameters uncertainty, e.g., line impedance and filter impedance variation. In specific, the rms value of measured total current harmonics at point of common coupling will be periodically sent to each inverter as feedback signal using the low-cost narrowband communication system. Then, the inverters will assume the R-P&O scheme to correct the phase shift angles among pulsewidth modulation carriers for intentionally minimizing the total current harmonics. Doing so, the closed-loop scheme can achieve the expected performance even under the severe parameters' variation. The experimental results verified the performance of the proposed method.**

***Index Terms*—Closed-loop control, global synchronous pulsewidth modulation (GSPWM), parallel-connected inverters, parameters uncertainty immunization.**

I. Introduction

THE voltage source inverters (VSIs) have been widely implemented in many applications, such as PV plants, wind plants, and battery energy storage stations, to integrate the distributed power sources to power grid [1]. The accumulated switching current harmonics at the point of common coupling (PCC) can be attenuated by assuming the interleaved pulsewidth modulation (PWM) sequences. Traditionally, the centralized PWM interleaving method can attenuate the current harmonics but is not adaptive to the distributed inverters [2], [3]. Some decentralized method can realize the carrier interleaving without using central controller but can only be used in dc converters [4], [5]. The recently proposed global synchronous PWM (GSPWM) method [6] provides a feasible operation scheme by coordinating the PWM sequences among paralleled VSIs. Besides, Xu *et al.* [7] and He *et al.* [8] proposed a phase-locked loop based carrier synchronization method for GSPWM, which significantly improves the operational adaptivity because it makes the GSPWM not rely on the low-latency communication channels.

Another important issue of PWM interleaving is the calculation of carrier phase shift angles. For inverters with totally identical parameters, the phase shift angles can be easily obtained [9]. For the inverters with different parameters, e.g., different inductance, output power, and switching frequencies, the GSPWM method can calculate their optimal phase shift angles to minimize the total current harmonics according to the preknown parameters [6], which is referred to the open-loop scheme. But in practice, some inverters' parameters cannot be measured accurately during operation, e.g., the filter impedance and the feeder impedance. As a consequence, the reported phase shift angle calculation methods, which merely assume the open-loop control principle, cannot exactly guarantee the high-frequency current harmonics attenuation as expected.

This letter therefore proposes a closed-loop scheme to guarantee the accurate harmonic attenuation by periodically capturing the rms value of total current harmonics and adjusting the carriers' phase shift angles discontinuously using the round perturbation and observation (R-P&O) method for GSPWM-VSIs. Doing so, the closed-loop scheme can achieve the wide adaptability in implementations even without knowing the accurate inverters' parameters. Experimental results verified the performance of the proposed scheme.

II. Performance Analysis of the Traditional Open-Loop GSPWM Scheme With Inaccurate Parameters

In this section, the performance of the traditional GSPWM operational principle will be briefly analyzed when the line parameters are not accurate in calculation.

In the following, N and m ($m = 1, \ldots, N$) indicate the quantity and the number of inverters, respectively. $\varphi_{m,\mathrm{PWM}}$ indicates the

Manuscript received February 11, 2020; revised March 6, 2020; accepted March 17, 2020. Date of publication March 22, 2020; date of current version July 20, 2020. This work was supported in part by the China Postdoctoral Science Foundation under Grants 2019TQ0183 and 2019M662358, in part by the National Natural Science Foundation of China under Grant 51722704, in part by the Shandong Provincial Natural Science Foundation, China, under Grant JQ201717, in part by the Foundation for Innovative Research Groups of National Natural Science Foundation of China under Grant 61821004, and in part by the Key Project of National Natural Science Foundation of China under Grant 61733010. *(Corresponding author: Feng Gao.)*

Tao Xu, Feng Gao, Pengfei Tan, and Xiangjian Meng are with the Key Lab of Power System Intelligent Dispatch and Control of Ministry of Education, Shandong University, Jinan 250061, China (e-mail: txu@sdu.edu.cn; fgao@sdu.edu.cn; 18765107094@163.com; el15xm@163.com).

Frede Blaabjerg is with the Department of Energy Technology, Aalborg University, 9100 Aalborg, Denmark (e-mail: fbl@et.aau.dk).

Color versions of one or more of the figures in this article are available online at http://ieeexplore.ieee.org.

Digital Object Identifier 10.1109/TPEL.2020.2982763

phase shift angle between PWM_m and PWM_1, where PWM_m and PWM_1 refer to the PWM sequences of inverters m and 1, respectively. The range of $\varphi_{m,\mathrm{PWM}}$ is from 0° to 360°. Besides, the variables with subscript c indicate the calculated values according to the theoretical model with inaccurate parameters. The variables with subscript a indicate the calculated values by employing the accurate parameters.

When using the open-loop scheme, the calculated optimal phase shift angle $\varphi_{m,\mathrm{PWM},c}$ is obtained by minimizing rms value of total current harmonics [6]

$$\begin{aligned} &\min \ I_{\mathrm{sum}h,c} \\ &= \sqrt{\sum_{f=f_0+1}^{\infty} \left| \sum_{m=1}^{N} I_{m,hf,c} e^{j\varphi_{m,hf}(\varphi_{m,\mathrm{PWM},c})} \right|^2} \\ &\text{s.t.} \ \ 0^\circ \le \varphi_{m,\mathrm{PWM},c} \le 360^\circ \\ &\dot{I}_{m,hf,c} = \frac{\dot{U}_{m,hf,c}}{Z_{m,\mathrm{out}}} \end{aligned} \tag{1}$$

where $I_{\mathrm{sum}h,c}$ indicates the calculated rms value of total current harmonics. $I_{m,hf,c}$ indicates the calculated rms value of harmonics flowing from inverter m with frequency f, which is derived according to harmonic voltage $\dot{U}_{m,hf,c}$ and the preknown output impedance $Z_{m,\mathrm{out}}$. $\dot{U}_{m,hf,c}$ can be derived using double Fourier method [10].

But in practice, $Z_{\mathrm{m,out}}$ contains the reactance of output filter and the estimated feeder impedance. The estimated feeder impedance is not always exactly equal to the real output impedance since the equivalent impedance under different high frequencies are totally different [11], [12] and affected by the ambient temperature. So, $\boldsymbol{\varphi_{\mathrm{PWM,c}}}$ which is the vector of all $\varphi_{m,\mathrm{PWM},c}$ is also not equal to the wanted accurate optimal phase angles $\boldsymbol{\varphi_{\mathrm{PWM,a}}}$ and the high-frequency harmonics of total current at PCC will not be minimized as expected. To clearly illustrate this phenomenon, a simple example with three inverters is assumed, where the inverters' parameters except the output impedance are assumed to be identical. The calculation model with inaccurate parameters is shown in Fig. 1(a). Fig. 1(c) illustrates $I_{\mathrm{sum}h,c}$ under all the possible combinations of $[\varphi_{1,PWM,c}, \varphi_{2,PWM,c}, \varphi_{3,PWM,c}]$, where the color in figure indicates the value of $I_{\mathrm{sum}h,c}$. $\varphi_{1,\mathrm{PWM}}$ is not shown here because it is set to 0° as the reference. The calculated $\boldsymbol{\varphi_{\mathrm{PWM,c}}}$ in this example is $[0^\circ, 120^\circ, 240^\circ]$. But after measuring the real filter value of each inverter, the accurate model is shown in Fig. 1(b). The measured $I_{\mathrm{sum}h,a}$ under different phase angle combinations are shown in Fig. 1(d), where $\boldsymbol{\varphi_{\mathrm{PWM,a}}}$ is $[0^\circ, 125^\circ, 222^\circ]$. It is obvious that $\boldsymbol{\varphi_{\mathrm{PWM,c}}}$ deviates from $\boldsymbol{\varphi_{\mathrm{PWM,a}}}$ because of the inaccurate parameters. If the inaccurate $\boldsymbol{\varphi_{\mathrm{PWM,c}}}$ is used in practice, $I_{\mathrm{sum}h,a}$ will be 0.316 A, as shown in Fig. 1(d), instead of the theoretically calculated 0.21 A in Fig. 1(c), though the real minimum value of $I_{\mathrm{sum}h,a}$ is 0.166 A. So, the existing open-loop scheme cannot track $I_{\mathrm{sum}h,a}$ properly when suffering the large parameter variation.

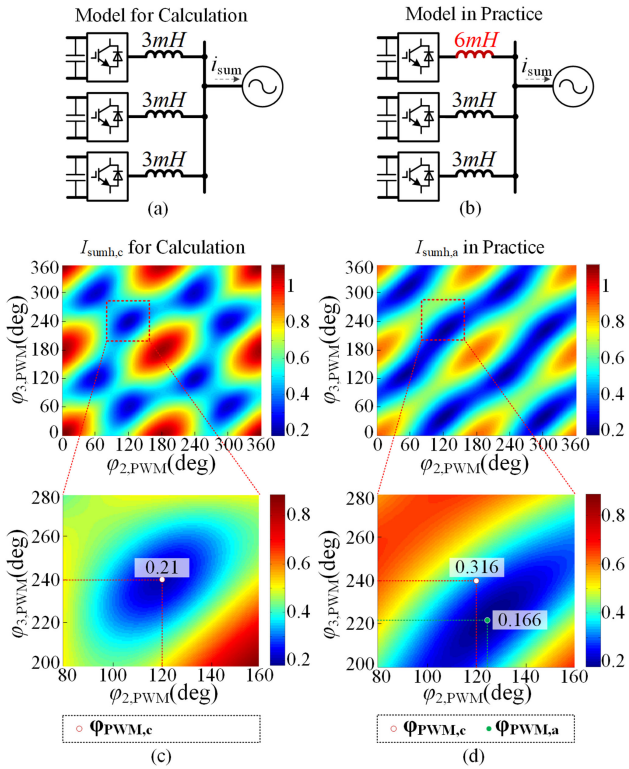

Fig. 1. Calculation models with (a) inaccurate and (b) accurate parameters, and (c) $I_{\mathrm{sum}h,c}$ and $\varphi_{m,\mathrm{PWM},c}$ in theory and (d) $I_{\mathrm{sum}h,a}$ and $\varphi_{m,\mathrm{PWM},a}$ in practice of three parallel-connected inverters.

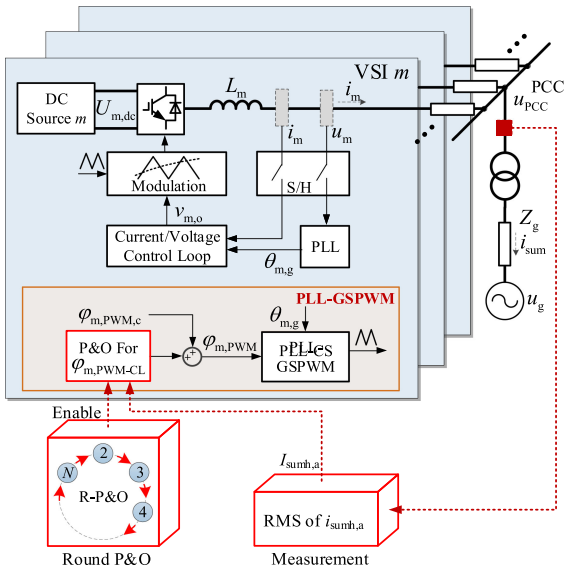

Fig. 2. Illustration of paralleled inverters with the proposed closed-loop scheme.

III. Principles and Realization of Closed-Loop Scheme

To improve the control accuracy when using GSPWM, the closed-loop scheme will be fully elaborated below. In principle, a measurement unit is used to sample $I_{\mathrm{sum}h,a}$ and send to each inverter, as shown in Fig. 2. Then, the coordination unit assumes the R-P&O algorithm to coordinate the switching sequences among inverters.

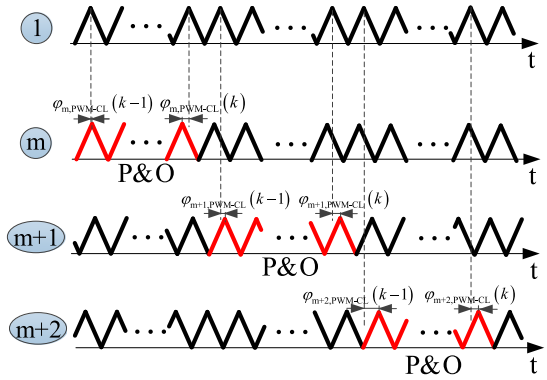

Fig. 3. Illustration of $\varphi_{m,\mathrm{PWM-CL}}$ using R-P&O.

In specific, a current sensor is installed to measure the total current harmonics $i_{\mathrm{sum}h,a}$ at PCC. Then, $I_{\mathrm{sum}h,a}$ can be simply derived and feedback to each inverter with the updating frequency f_{CL}. Since $I_{\mathrm{sum}h,a}$ is a specific value, it can be easily transmitted using the low-cost narrowband communication system. To be noted, the switching harmonics can be easily sampled because the sampling frequency could be set up to several hundred kilohertz. Upon inverters receive $I_{\mathrm{sum}h,a}$, $I_{\mathrm{sum}h,a}$ will be employed as the feedback value to generate the compensating phase shift angles to correct $\varphi_{m,\mathrm{PWM}}$ as

$$\varphi_{m,\mathrm{PWM}} = \varphi_{m,\mathrm{PWM},c} + \varphi_{m,\mathrm{PWM-CL}} \tag{2}$$

where $\varphi_{m,\mathrm{PWM-CL}}$ indicates the compensating phase shift angles for inverter m. $\varphi_{1,\mathrm{PWM\text{-}CL}}$ is still set as 0°. Doing so, $I_{\mathrm{sum}h,a}$ is given as

$$I_{\mathrm{sum}h,a} = \sqrt{\sum_{f=f_0+1}^{\infty}\left|\sum_{m=1}^{N} I_{m,hf,a}e^{j\varphi_{m,hf,a}(\varphi_{m,\mathrm{PWM},a}+\varphi_{m,\mathrm{PWM-CL}})}\right|^2}. \tag{3}$$

Compared with the model built in (1), $\varphi_{m,\mathrm{PWM-CL}}$ cannot be directly calculated by minimizing $I_{\mathrm{sum}h,a}$ because the parameters in (3), such as $I_{m,hf,a}$, cannot be obtained accurately. So, the perturbation and observation method can be assumed to find the optimal $\varphi_{m,\mathrm{PWM-CL}}$. According to the model of (3), $I_{\mathrm{sum}h,a}$ is determined by $\varphi_{m,\mathrm{PWM-CL}}$ of all inverters. That means, if all the inverters operate P&O together, it will be hard for each inverter to determine the changing direction of $\varphi_{m,\mathrm{PWM-CL}}$.

In order to find $\varphi_{m,\mathrm{PWM-CL}}$, the R-P&O scheme is proposed, which only perturbates one $\varphi_{m,\mathrm{PWM-CL}}$ each time, as shown in Fig. 3. When using the R-P&O, $I_{\mathrm{sum}h,a}$ is given as

$$I_{\mathrm{sum}h,a}\begin{pmatrix}\varphi_{m,\mathrm{PWM-CL}}\\ \pm\Delta\varphi_{m,\mathrm{PWM-CL}}\end{pmatrix} = \sqrt{\sum_{f=f_0+1}^{\infty}\left|\begin{matrix}I_{m,hf,a}e^{j\varphi_{m,hf,a}[\varphi_{m,\mathrm{PWM},c}+\varphi_{m,\mathrm{PWM-CL}}(k)]}\\ +\sum_{\substack{i=1\\ i\neq m}}^{N} I_{\mathrm{i},hf,a}e^{j\varphi_{i,hf,a}(\varphi_{i,\mathrm{PWM},c}+\varphi_{i,\mathrm{PWM-CL}})}\end{matrix}\right|^2} \tag{4}$$

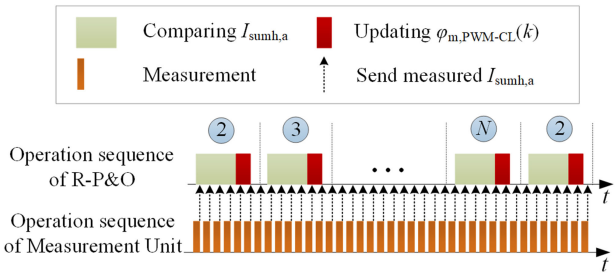

Fig. 4. Operation sequences of R-P&O and measurement unit when the proposed closed-loop scheme is employed.

where $I_{\mathrm{sum}h,a}$ is dependent on $\varphi_{m,\mathrm{PWM-CL}}(k)$ because other $\varphi_{i,\mathrm{PWM-CL}}(i \neq m)$ are unchanged. The perturbation will begin with the initial $\varphi_{m,\mathrm{PWM-CL}}(0)$ being 0°. In order to determine the updating direction of $\varphi_{m,\mathrm{PWM-CL}}(k)$, $\varphi_{m,\mathrm{PWM-CL}}(k)$ is perturbated to the following three values one after another:

$$\begin{aligned}\varphi_{m,\mathrm{PWM-CL}}(k) &= \varphi_{m,\mathrm{PWM-CL}}(k-1)\\ \varphi_{m,\mathrm{PWM-CL}}(k) &= \varphi_{m,\mathrm{PWM-CL}}(k-1) + \Delta\varphi_{m,\mathrm{PWM-CL}}\\ \varphi_{m,\mathrm{PWM-CL}}(k) &= \varphi_{m,\mathrm{PWM-CL}}(k-1) - \Delta\varphi_{m,\mathrm{PWM-CL}}\end{aligned} \tag{5}$$

where $\triangle\varphi_{m,\mathrm{PWM-CL}}$ indicates the perturbation step. During the perturbation, the measurement unit measures $I_{\mathrm{sum}h,a}$ and sends $I_{\mathrm{sum}h,a}$ to inverter m. Then, inverter m can update $\varphi_{m,\mathrm{PWM-CL}}(k)$ to the value who leads to the minimum $I_{\mathrm{sum}h,a}$. The $\varphi_{m,\mathrm{PWM-CL}}(k)$ is updated one time during each P&O operation, then the P&O operation will be triggered in inverter m+1. After finishing P&O operation for inverter N, the P&O will be employed again from inverter 2 to inverter N and repeat the aforementioned procedures. The sequence diagram of the closed-loop scheme is shown in Fig. 4, where the measurement operates all the time while P&O operates from one inverter to next inverter.

The example with three inverters shown in Fig. 1(b) is still employed here to briefly illustrate the closed-loop scheme. The calculated $\varphi_{\mathbf{PWM,c}}$ is $[0^\circ, 120^\circ, 240^\circ]$ and the initial $\varphi_{m,\mathrm{PWM-CL}}(0)$ is 0°. $\triangle\varphi_{m,\mathrm{PWM-CL}}$ is assumed as 5°. First, only $\varphi_{2,\mathrm{PWM\text{-}CL}}$ is perturbated while $\varphi_{3,\mathrm{PWM\text{-}CL}}$ is fixed at 0°, as shown in the left-hand side figure of Fig. 5(a). After comparing $I_{\mathrm{sum}h,a}$ for $\varphi_{2,\mathrm{PWM\text{-}CL}} = -5^\circ, 0^\circ, +5^\circ$, inverter 2 updates $\varphi_{2,\mathrm{PWM\text{-}CL}}$ to $+5^\circ$ who produces the minimum $I_{\mathrm{sum}h,a}$. The right-hand side figure of Fig. 5(a) shows the updating trajectory of $\varphi_{2,\mathrm{PWM\text{-}CL}}$. Then, only $\varphi_{3,\mathrm{PWM\text{-}CL}}$ is perturbated while the $\varphi_{2,\mathrm{PWM\text{-}CL}}$ is fixed at 5°, as shown in the left-hand side figure of Fig. 5(b). Being similar to the P&O procedures for $\varphi_{2,\mathrm{PWM\text{-}CL}}$, the $\varphi_{3,\mathrm{PWM\text{-}CL}}$ is updated as -5°. The right-hand side figure of Fig. 5(b) shows the updating trajectory of $\varphi_{3,\mathrm{PWM\text{-}CL}}$. Then, repeating P&O for inverters 2 and 3, $I_{\mathrm{sumh,a}}$ will approach the real minimum value, as shown in Fig. 5(c).

To avoid the locally optimal solutions, $\varphi_{m,\mathrm{PWM,c}}$ should be precalculated. Fortunately, $\varphi_{m,\mathrm{PWM},c}$ is close to $\varphi_{m,\mathrm{PWM},a}$, which can help the round P&O algorithm to track the optimal values. Then, the round P&O with variable steps can be used.

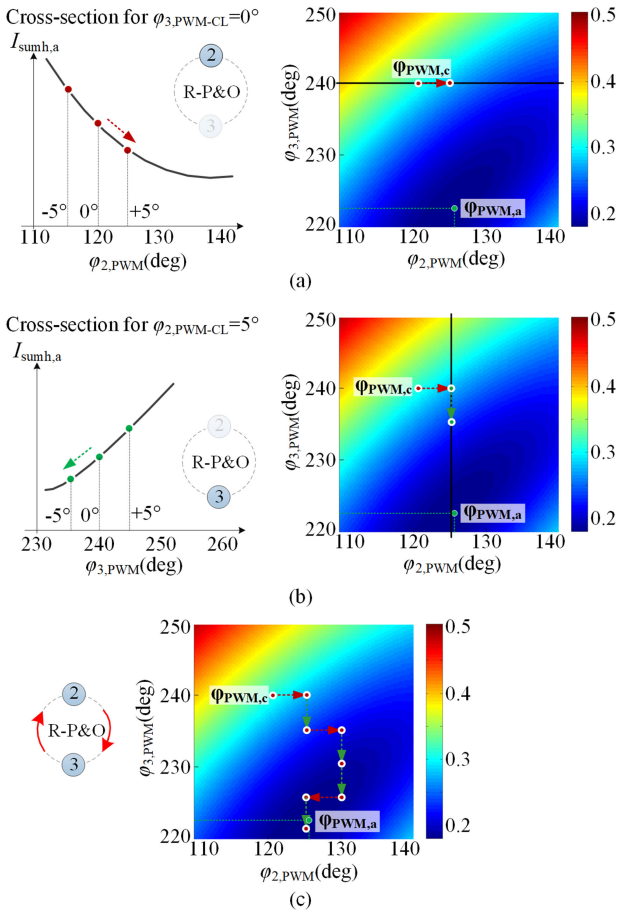

Fig. 5. Illustration of R-P&O for three inverters. (a) When only perturbate $\varphi_{2,\mathrm{PWM\text{-}CL}}$ while keep $\varphi_{3,\mathrm{PWM\text{-}CL}}$ fixed. (b) When only perturbate $\varphi_{3,\mathrm{PWM\text{-}CL}}$ while keep $\varphi_{2,\mathrm{PWM\text{-}CL}}$ fixed. (c) Whole trajectory of $\varphi_{m,\mathrm{PWM}}$.

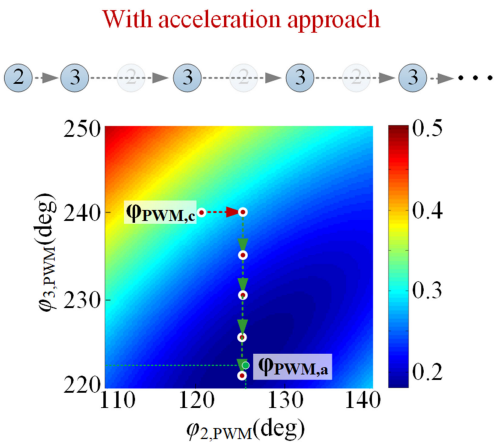

Fig. 6. Trajectory of $\varphi_{m,\mathrm{PWM}}$ for three inverters with acceleration approach.

In principle, the variable steps are set as large value initially and then decrease [13]–[15].

On the other hand, in order to reduce the tracking time when the number of inverter is large, the sequences of P&O operation can be rearranged according to the gradient of last P&O operation. The gradients of $I_{\mathrm{sum},h,a}$ when using P&O operation in different inverters are calculated and compared. Then,

TABLE I
EXPERIMENTAL PARAMETERS

m	$U_{\mathrm{m,dc}}$/V	L_{m}/mH	$f_{\mathrm{m,c}}$
1	170 V	6 mH	10 kHz
2	165 V	3 mH	10 kHz
3	168 V	3 mH	10 kHz

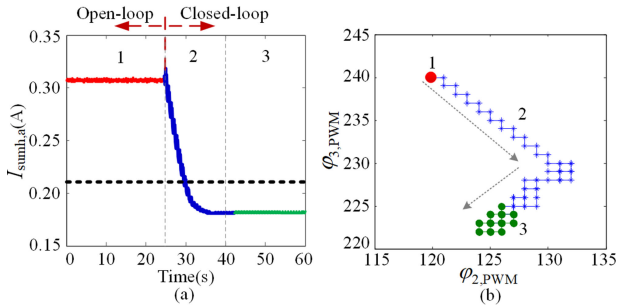

Fig. 7. (a) Trajectory of $I_{\mathrm{sum}h,a}$. (b) Trajectory of $\varphi_{m,\mathrm{PWM}}$.

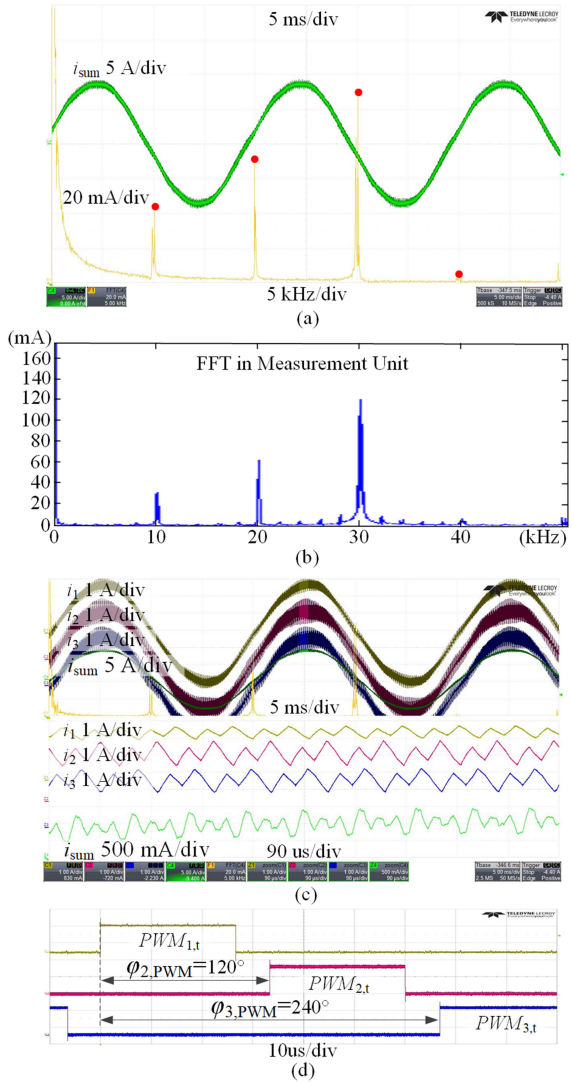

Fig. 8. Experimental waveforms of OL-GSPWM with (a) $I_{\mathrm{sum}h,a}$ and FFT spectrum, (b) FFT results in measurement unit, (c) i_1, i_2, i_3, $i_{\mathrm{sum}h,a}$ and the zoomed view, and (d) measured $\varphi_{m,\mathrm{PWM}}$.

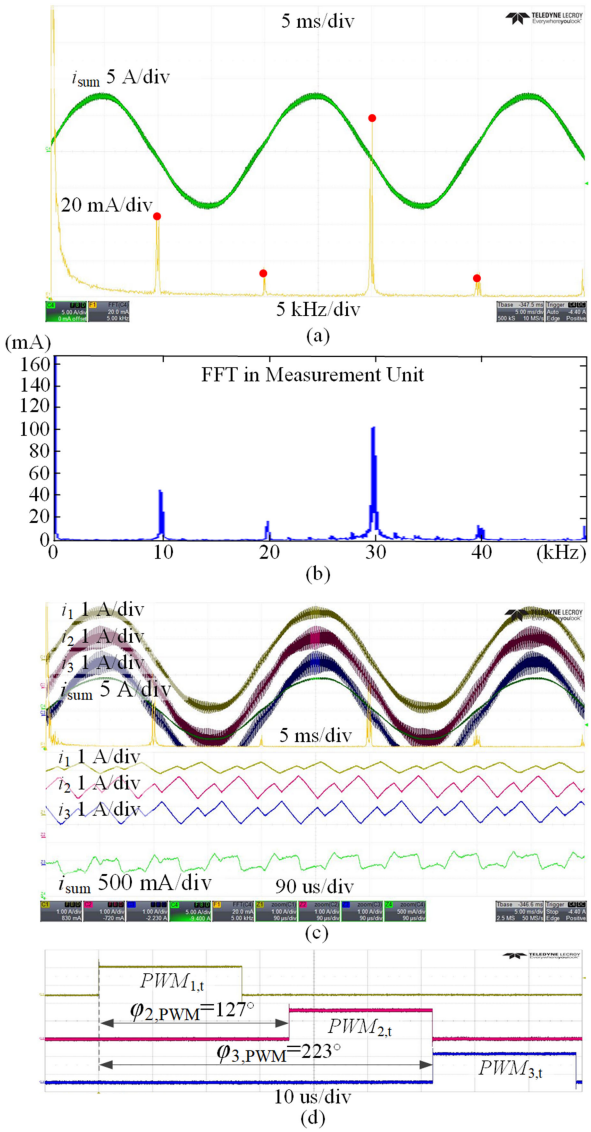

Fig. 9. Experimental waveforms of CL-GSPWM with (a) $I_{\mathrm{sum}h,a}$ and FFT spectrum, (b) FFT results in measurement unit, (c) i_1, i_2, i_3, $i_{\mathrm{sum}h,a}$ and the zoomed view, and (d) measured $\varphi_{m,\mathrm{PWM}}$.

the inverter whose last P&O operation leads to the maximum gradient will be enabled. Fig. 6 shows the trajectory of $\varphi_{m,\mathrm{PWM}}$ with this kind of acceleration approach. The gradients of last P&O operation in inverter 2 and inverter 3 are compared. The P&O operation in inverter 3 leads to larger gradient, so the P&O algorithm will run again in inverter 3. Comparing Figs. 5(c) and 6, the superiority of acceleration procedure is obvious.

IV. Experimental Verification

The constructed experimental prototype has three three-phase two-level VSIs with their own independent dc sources, output filters, and digital controllers. The used DSP is TMS320F28335. The inverter parameters are listed in Table I. All inverters are connected to an emulated grid using a programmable ac source, whose rms value of output voltage is 110 V and the rated output frequency is 50 Hz. The oscilloscope with four channels was used to record the waveforms. A measurement unit containing DSP and sensor board was used to measure and calculate $I_{\mathrm{sum}h}$. First, the total current i_{sum} is measured and converted into low-voltage signal by Hall sensor (LA100-P) and amplifier within the range of 0–3 V. Then, the analog signal is converted into digital signal by the analog-to-digital converter (ADC) module of DSP (TMS320F28335). The sampling rate of ADC module is 102.4 kHz. A radix-2 fast Fourier transform (FFT) algorithm is running in this DSP, which converts the current samples to frequency domain after sampling 20 ms. Finally, $I_{\mathrm{sum}h,a}$ can be easily derived according to the FFT results. $I_{\mathrm{sum}h,a}$ will be sent to each inverter through the RS-485 communication channels in this experiment. The updating frequency of the measurement unit is set as 10 Hz.

In this experiment, the open-loop scheme is used from 0 to 25 s and the proposed closed-loop scheme is assumed from 25 to 60 s. Fig. 7 shows the trajectories of $I_{\mathrm{sum}h,a}$ and $\varphi_{m,\mathrm{PWM}}$. The trajectories are divided into three stages. In stage 1, the calculated $I_{\mathrm{sum}h,c}$ is 0.21 A and the calculated $\boldsymbol{\varphi_{\mathrm{PWM,c}}}$ is $[0°, 120°, 240°]$ in theory. But when employing $\boldsymbol{\varphi_{\mathrm{PWM,c}}}$ in open-loop GSPWM, the measured $I_{\mathrm{sum}h,a}$ is actually 0.31 A. That means the open-loop scheme underestimates the current harmonics and cannot control $I_{\mathrm{sum}h,a}$ accurately. After using the proposed closed-loop scheme, $\boldsymbol{\varphi_{\mathrm{PWM}}}$ will change to $[0°, 127°, 223°]$ because $\varphi_{m,\mathrm{PWM-CL}}$ is used to compensate $\boldsymbol{\varphi_{\mathrm{PWM}}}$, as shown in stage 2. After 10 s, the measured $I_{\mathrm{sum}h,a}$ becomes 0.18 A, which approaches the minimum value, as shown in stage 3.

Fig. 8 shows the experimental waveforms of the open-loop scheme in stage 1, whereas Fig. 9 shows the experimental waveforms of the closed-loop scheme in stage 3. Comparing the experimental results of open-loop scheme and closed-loop scheme, it is noted that the closed-loop scheme can approach the real minimum value. Besides, the FFT spectrum in Figs. 8 and 9 verified that the FFT results in measurement unit are equal to those calculated by the oscilloscope whose sampling frequency can be up to 50 MHz. So, the measurement unit is able to measure $I_{\mathrm{sum}h,a}$ in practice.

V. Conclusion

This letter proposes a closed-loop GSPWM scheme with R-P&O algorithm for paralleled VSIs to immunize the parameters uncertainty. Experimental results verified the performance of the proposed method.

References

[1] F. Blaabjerg, Z. Chen, and S. B. Kjaer, "Power electronics as efficient interface in dispersed power generation systems," *IEEE Trans. Power Electron.*, vol. 19, no. 5, pp. 1184–1194, Sep. 2004.

[2] M. A. Abusara and S. M. Sharkh, "Design and control of a grid-connected interleaved inverter," *IEEE Trans. Power Electron.*, vol. 28, no. 2, pp. 748–764, Feb. 2013.

[3] D. Zhang, F. Wang, R. Burgos, R. Lai, and D. Boroyevich, "Impact of interleaving on AC passive components of paralleled three-phase voltage-source converters," *IEEE Trans. Ind. Appl.*, vol. 46, no. 3, pp. 1042–1054, May/Jun. 2010.

[4] M. Sinha, J. Poon, B. B. Johnson, M. Rodriguez, and S. V. Dhople, "Decentralized interleaving of parallel-connected buck converters," *IEEE Trans. Power Electron.*, vol. 34, no. 5, pp. 4993–5006, May 2019.

[5] D. Perreault and J. Kassakian, "Distributed interleaving of paralleled power converters," *IEEE Trans. Circuits Syst. I, Fundam. Theory Appl.*, vol. 44, no. 8, pp. 728–734, Aug. 1997.

[6] T. Xu and F. Gao, "Global synchronous pulse width modulation of distributed inverters," *IEEE Trans. Power Electron.*, vol. 31, no. 9, pp. 6237–6253, Sep. 2016.

[7] T. Xu, F. Gao, X. Wang, and F. Blaabjerg, "A carrier synchronization method for global synchronous pulse width modulation application using phase-locked-loop," *IEEE Trans. Power Electron.*, vol. 34, no. 11, pp. 10720–10732, Nov. 2019.

[8] J. He, Z. Dong, Y. Li, and C. Wang, "Parallel-converter system grid current switching ripples reduction using a simple decentralized interleaving PWM approach," *IEEE Trans. Power Electron.*, 2019, to be published.

[9] B. Cougo, T. Meynard, and G. Gateau, "Parallel three-phase inverters: Optimal PWM method for flux reduction in intercell transformers," *IEEE Trans. Power Electron.*, vol. 26, no. 8, pp. 2184–2191, Aug. 2011.

[10] D. G. Holmes and T. A. Lipo, *Pulse Width Modulation for Power Converters: Principles and Practice*. New York, NY, USA: Wiley, 2003, pp. 241–249.

[11] S. Morched and P. Kundur, "Identification and modelling of load characteristics at high frequencies," *IEEE Trans. Power Syst.*, vol. 2, no. 1, pp. 153–159, Feb. 1987.

[12] A. Girgis and R. B. McManis, "Frequency domain techniques for modeling distribution or transmission networks using capacitor switching induced transients," *IEEE Trans. Power Del.*, vol. 4, no. 3, pp. 1882–1890, Jul. 1989.

[13] J. Ahmed and Z. Salam, "An enhanced adaptive P&O MPPT for fast and efficient tracking under varying environmental conditions," *IEEE Trans. Sustain. Energy*, vol. 9, no. 3, pp. 1487–1496, Jul. 2018.

[14] J. Prasanth Ram and N. Rajasekar, "A novel flower pollination based global maximum power point method for solar maximum power point tracking," *IEEE Trans. Power Electron.*, vol. 32, no. 11, pp. 8486–8499, Nov. 2017.

[15] W. Zhang, G. Zhou, H. Ni, and Y. Sun, "A modified hybrid maximum power point tracking method for photovoltaic arrays under partially shading condition," *IEEE Access*, vol. 7, pp. 160091–160100, 2019.